

Self-similar collapse with cooling and heating in an expanding universe

Shuji Uchida and Tatsuo Yoshida

Faculty of Science, Ibaraki University, 2-1-1 Bunkyo, Mito, Ibaraki, 310-8512, Japan

Accepted ****. Received ****, in original form ****

ABSTRACT

We derive self-similar solutions including cooling and heating in an Einstein de-Sitter universe, and investigate the effects of cooling and heating on the gas density and temperature distributions. We assume that the cooling rate has a power-law dependence on the gas density and temperature, $\Lambda \propto \rho^A T^B$, and the heating rate is $\Gamma \propto \rho T$. The values of A and B are chosen by requiring that the cooling time is proportional to the Hubble time in order to obtain similarity solutions. In the region where the cooling rate is greater than the heating rate, a cooling inflow is established, and the gas is compressed and heats up. Because the compression is greater in the inner region than in the outer region, the temperature becomes an increasing profile toward the center. In particular, when a large infall velocity is produced due to an enormous energy loss, the slope of the density approaches a value that depends on A , B , and the velocity slope, and the slope of the temperature approaches -1 . On the other hand, in the region where the heating rate is greater than the cooling rate, the infall velocity is suppressed, compression of the gas is weakened, and the gas cools down. The slope of the density becomes shallow due to suppression of the contraction, and the temperature is lower than that without heating. The self-similar collapse presented here gives insights to the effects of cooling and heating on the gas distributions in galaxies and clusters of galaxies.

Key words: cosmology: theory - galaxies: clusters: general - gravitation - hydrodynamics - intergalactic medium - methods: analytical - radiation mechanisms: general.

1 INTRODUCTION

Clusters of galaxies contain large quantities of hot gas. The gas collapses under the influence of gravity, and loses thermal energy due to radiative cooling. Especially, the effect of cooling is important in the inner region where the cooling time is less than the Hubble time. Inside this region, it is expected that the internal pressure decreases, the gas cools down and cooling flows occur. However, from recent observations of clusters of galaxies, the expected cooled gas is not detected in the central region (Peterson et al. 2001; Tamura et al. 2001). Furthermore, X-ray observations indicate that the observed luminosity-temperature relation differs from the self-similar relation (Arnaud & Evrard 1999; Helsdon & Ponman 2000). As an origin of this discrepancy, it is supported that the gas is significantly affected by non-gravitational heating (Kaiser 1991; Evrard & Henry 1991). It is very important to investigate the influences of cooling and heating on the gas distributions, and it would provide an understanding of the thermal evolution of the intracluster medium.

For adiabatic similarity solutions in an Einstein de-

Sitter universe, Bertschinger(1985) derived the similarity solution of a top-hat density perturbation, $n=3$, where n is a power spectrum index, and showed that the density has a power-law profile against the radius, $\rho \propto r^{-2.25}$. Chuzhoy & Nusser(2000) obtained the asymptotic behaviour of similarity variables of adiabatic gas, and found that they strongly depend on the initial power spectrum. For $n > -2$, they found that the density and temperature asymptotically approach $\rho \propto r^{-3(n+3)/(n+5)}$ and $T \propto r^{-(n-1)/(n+5)}$ in the limit $r \rightarrow 0$, respectively. For a self-similar solution with cooling, Abadi et al.(2000) obtained a similarity solution of collisional gas in an Einstein de-Sitter universe, and used it to evaluate the ability of SPH simulations. In their solution, they assumed the cooling function $\Lambda \propto \rho^{3/2} T$. This power-law dependence is determined by the requirement that the cooling time must have a fixed fraction to the dynamical time in order to obtain the similarity solution. They found that radiative cooling decreases the pressure support, and establishes a cooling inflow. As a result, the profiles of fluid variables differ from those of the adiabatic solution. In particular, when the energy loss is large enough to produce a

large infall velocity, they found that the density and temperature approach $\rho \propto r^{-2}$ and $T \propto r^{-1}$ as $r \rightarrow 0$, respectively.

The purpose of this study is to investigate the effects of cooling and heating on the gas distributions using the similarity solution. The cooling rate per unit volume is assumed to be given by the power-law dependences on the density and temperature, $\Lambda \propto \rho^A T^B$, where A and B are related to the initial power spectrum. The heating rate is assumed to be proportional to the gas density and temperature, $\Gamma \propto \rho T$. Of course, the similarity solution is not directly applicable to the real structure, and cannot include detailed physical processes. However, it is possible to show exact structures of flows and to give clues concerning the effects of cooling and heating on the gas distributions of galaxies and clusters of galaxies.

The layout of the paper is as follows. In Section 2, we present our model. Our results are shown in Section 3. Finally, we discuss and summarize our results in Section 4.

2 MODEL

2.1 Spherical collapse in an expanding universe

We consider here that an over-dense region has a density contrast (δ_i) at an initial Hubble time of $t_{H,i}$, and that the background universe is an Einstein de-Sitter universe. The gravitational collapse in the flat universe becomes a similarity evolution because bounded shells extend to infinity. Fillmore & Goldreich(1984) introduced a scale-free initial density contrast,

$$\delta_i = \frac{\delta M_i}{M_i} = \left(\frac{M_i}{M_0}\right)^{-\epsilon} = \left(\frac{r_i}{R_0}\right)^{-3\epsilon}, \quad (1)$$

where $M_i = (4/3)\pi\rho_{H,i}r_i^3$ is the mass contained within the proper radius r_i , $\rho_{H,i} = 1/(6\pi G t_{H,i}^2)$ is the background density at $t_{H,i}$, and $M_0 = (4/3)\pi\rho_{H,i}R_0^3$ is a reference mass. Since δM_i must be constant or increase with increasing radius, and δ_i has to decrease with increasing radius, ϵ is restricted to $0 < \epsilon \leq 1$. The variance of the density fluctuation is

$$|\delta(x, t_H)|^2 \simeq k^3 |\delta_k|^2 \simeq a(t_H)^2 M^{-\frac{n+3}{3}}, \quad (2)$$

where x is the comoving radius, and $|\delta_k|^2 \propto a(t_H)^2 k^n$ is the power spectrum, where $a(t_H)$ is an expansion factor. The relation between the index n and the parameter ϵ is

$$n = 3(2\epsilon - 1). \quad (3)$$

We assume that the initial velocity of matter is pure Hubble flow, and that the initial gas pressure is zero. The expanding matter slows down with the growth of the perturbation. Eventually, it reaches a maximum radius and decouples from the Hubble expansion. Since $a(t_H) \propto t_H^{2/3}$, the perturbation grows as $|\delta(r, t_H)|^2 \propto a(t_H)^{n+5} r^{-(n+3)} \propto t_H^{2(n+5)/3} r^{-(n+3)}$, based on equation (2). The density contrast at the turn-around radius is $\delta(r_{ta}, t_H) = (3\pi/4)^2 - 1 \sim 4.55$ (Peebles 1980). Thus, the time evolution of the turn-around radius and the enclosed mass are

$$r_{ta}(t_H) \propto t_H^\xi, \quad (4)$$

$$m_{ta}(t_H) \propto t_H^{\frac{2}{3\epsilon}}, \quad (5)$$

where

$$\xi = \frac{2}{3}(1 + \frac{1}{3\epsilon}). \quad (6)$$

After the turn-around, particles fall toward the center. The collapse of matter causes an increase of the central density. Since the gas particles are decelerated, a shock wave is formed and propagates outward. The system undergoes self-similar evolution at a later time.

2.2 Cooling and heating laws in similarity evolutions

In the case of the collapse of adiabatic gas, the physical scale of the system is only determined by the gravitational dynamics. When radiative cooling and heating are included, the similarity evolution is broken due to the existence of many physical scales. In order to maintain the similarity evolution, it is required that all of the physical scales are proportional to the dynamical scale. The scale-free condition was constructed by ensuring that the cooling time is proportional to the dynamical time (Owen et al. 1998; Abadi et al. 2000).

We assume that the cooling rate per unit volume is $\Lambda = \Lambda_0 \rho^A c_s^{2B}$. Here, A and B are free parameters, Λ_0 is the cooling coefficient, ρ is the gas density, and c_s is the sound speed. The cooling time becomes

$$t_{cool} = \frac{E}{\frac{DE}{Dt}} = E \left(\frac{\Lambda}{\rho}\right)^{-1} = \frac{\rho^{1-A} c_s^{2(1-B)}}{\gamma(\gamma-1)\Lambda_0}, \quad (7)$$

where E is the specific thermal energy of the gas, and $\gamma = 5/3$ is the adiabatic index. The Hubble time evolves as

$$t_H = \frac{2}{3} H_0^{-1} \left(\frac{a}{a_0}\right)^{\frac{3}{2}}, \quad (8)$$

where a_0 and H_0 are the expansion factor and Hubble constant at the present epoch, respectively. The sound speed and density evolve as

$$c_s = \left(\frac{a}{a_0}\right)^{\frac{1-n}{2(3+n)}} c_{s,0}, \quad (9)$$

$$\rho = \left(\frac{a}{a_0}\right)^{-3} \rho_0, \quad (10)$$

where $c_{s,0}$ and ρ_0 are the sound speed and the gas density at the present epoch, respectively. We assume that the Hubble time is proportional to the cooling time by the constant \hat{t}_c , in order to maintain scale-free conditions (i.e., $t_H = \hat{t}_c t_{cool}$),

$$t_H = \hat{t}_c \frac{\rho^{1-A} c_s^{2(1-B)}}{\gamma(\gamma-1)\Lambda_0}. \quad (11)$$

Substituting equations (8)-(10), the above equation becomes

$$\frac{2}{3} H_0^{-1} \left(\frac{a}{a_0}\right)^{\frac{3}{2}-3(A-1)-\frac{1-n}{3+n}(1-B)} = \hat{t}_c \frac{\rho_0^{1-A} c_{s,0}^{2(1-B)}}{\gamma(\gamma-1)\Lambda_0}. \quad (12)$$

The a -dependence term must vanish in order to keep \hat{t}_c constant. Using equation (3), we find

$$\frac{3}{2} - 3(A-1) - \frac{2-3\epsilon}{3\epsilon}(1-B) = 0. \quad (13)$$

Figure 1 displays the parameter space of A and B in relation to ϵ . The shaded areas correspond to $0 < \epsilon \leq 1$. The solid lines display the lines of $\epsilon=1$, $2/3$, $1/3$, and 0 . Abadi et al.(2000) selected at the point $(A,B)=(3/2,1)$, which is independent of ϵ . The points of free-free emission,

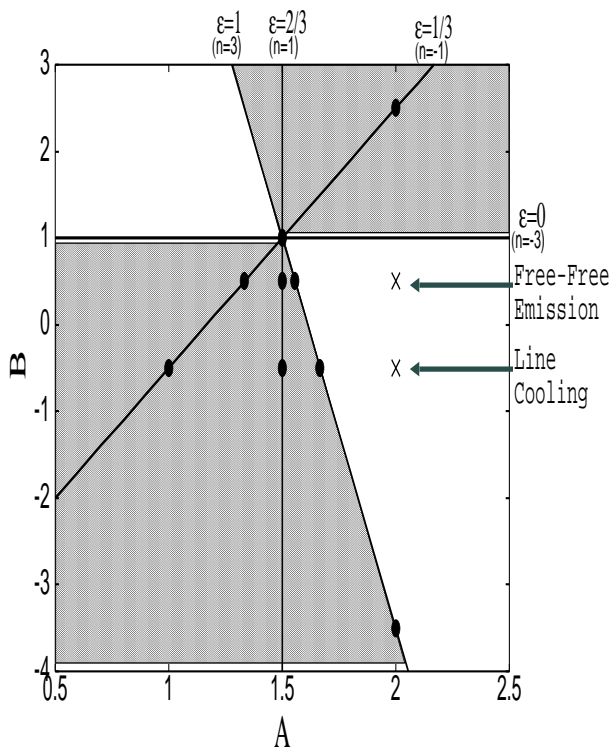


Figure 1. Relation between (A, B) and ϵ . The shaded areas indicate the inside of the range $0 < \epsilon \leq 1$. The solid lines are constant values of $\epsilon=1, 2/3, 1/3$, and 0. The closed circles represent the parameter positions that we calculated in this paper. The points of free-free emission and line cooling are indicated by crosses.

$(A, B)=(2, 1/2)$, and line cooling, $(A, B)=(2, -1/2)$, are indicated by crosses.

Next, we assume that the heating rate per unit volume is given by

$$\Gamma = \alpha \rho c_s^2, \quad (14)$$

where $\alpha=(t_{H,0}/t_H)\alpha_0$, $t_{H,0}$ is the current Hubble time, and α_0 is the model parameter. The heating time becomes

$$t_{heat} = \frac{E}{\frac{DE}{Dt}} = E\left(\frac{\Gamma}{\rho}\right)^{-1} = \frac{1}{\gamma(\gamma-1)} \frac{1}{\alpha}. \quad (15)$$

We assume that the heating time is proportional to the Hubble time by the constant t_h (i.e., $t_H=t_h t_{heat}$),

$$\frac{2}{3}H_0^{-1} = \frac{t_h}{\gamma(\gamma-1)\alpha_0}. \quad (16)$$

2.3 Basic equations of collisional gas

Neglecting the effect of dark matter, the basic equations with additional terms of cooling and heating are as follows:

$$\frac{\partial m}{\partial r} = 4\pi r^2 \rho, \quad (17)$$

$$\frac{\partial \rho}{\partial t} + \frac{1}{r^2} \frac{\partial}{\partial r} (r^2 \rho v) = 0, \quad (18)$$

$$\frac{\partial v}{\partial t} + v \frac{\partial v}{\partial r} = -\frac{\partial}{\gamma \rho \partial r} (\rho c_s^2) - \frac{Gm}{r^2}, \quad (19)$$

$$\frac{1}{\gamma-1} \frac{dc_s^2}{dt} - \frac{c_s^2}{\rho} \frac{d\rho}{dt} = -\gamma \Lambda_0 \rho^{A-1} c_s^{2B} + \gamma \alpha c_s^2, \quad (20)$$

where v is the velocity, G is the gravitational constant, and m is the mass of the gas.

To derive self-similar solutions, we introduce the similarity variable X and similarity functions, which are given by the following forms:

$$X = \frac{r}{r_{ta}}, \quad (21)$$

$$\rho = \rho_H D, \quad (22)$$

$$v = \frac{r_{ta}}{t_H} V, \quad (23)$$

$$c_s = \frac{r_{ta}}{t_H} C, \quad (24)$$

$$m = \frac{4}{3} \pi \rho_H r_{ta}^3 M, \quad (25)$$

$$\alpha = \frac{\mathcal{H}}{t_H}, \quad (26)$$

where $\rho_H=1/(6\pi G t_H^2)$ is the mean density of the universe, and \mathcal{H} is the same as $\alpha_0 t_{H,0}$ or $3H_0 t_h t_{H,0}/2\gamma(\gamma-1)$ from equation (16). The density and the sound speed are expressed as

$$\rho = \rho_0 \frac{\rho_H}{\rho_{H,0}}, \quad (27)$$

$$c_s = c_{s,0} \left(\frac{r_{ta}}{t_H}\right) \left(\frac{r_{ta,0}}{t_{H,0}}\right), \quad (28)$$

where $\rho_{H,0}$ and $r_{ta,0}$ are the background density and the turn-around radius at the present epoch, respectively. We substitute equations (27) and (28) for (11), and define Λ_0 as

$$\begin{aligned} \Lambda_0 &= \frac{t_c \left(\frac{\rho_0}{\rho_{H,0}}\right)^{1-A} \left(\frac{c_{s,0} t_{H,0}}{r_{ta,0}}\right)^{2(1-B)}}{\gamma(\gamma-1)} \rho_H^{1-A} r_{ta}^{2(1-B)} t_H^{2B-3}, \\ &= \frac{K_0}{\gamma(\gamma-1)} \rho_H^{1-A} r_{ta}^{2(1-B)} t_H^{2B-3}. \end{aligned} \quad (29)$$

Substituting equations (21)-(26), and (29) for (17)-(20), the fluid equations become,

$$\frac{dM}{dX} = 3X^2 D, \quad (30)$$

$$(V - \xi X) \frac{dD}{dX} + D \frac{dV}{dX} + 2D \left(\frac{V}{X} - 1\right) = 0, \quad (31)$$

$$(V - \xi X) \frac{dV}{dX} - (1 - \xi)V = -\frac{1}{\gamma D} \frac{d}{dX} (DC^2) - \frac{2M}{9X^2}, \quad (32)$$

$$\begin{aligned} \frac{2}{\gamma-1} [(\xi-1) + \frac{(V-\xi X)}{C} \frac{dC}{dX}] + 2 - \frac{(V-\xi X)}{D} \frac{dD}{dX} \\ = -\frac{K_0}{(\gamma-1)} D^{A-1} C^{2B-2} + \gamma \mathcal{H}. \end{aligned} \quad (33)$$

The non-dimensional mass M is derived by another integration (Bertschinger 1985). The equation of continuity is rewritten as follows:

$$\frac{\partial m}{\partial t} + 4\pi r^2 \rho v = 0. \quad (34)$$

Substituting equations (21)-(25) for (17) and (34), the dimensionless mass is

$$M = \frac{-3}{3\xi-2} X^2 D (V - \xi X). \quad (35)$$

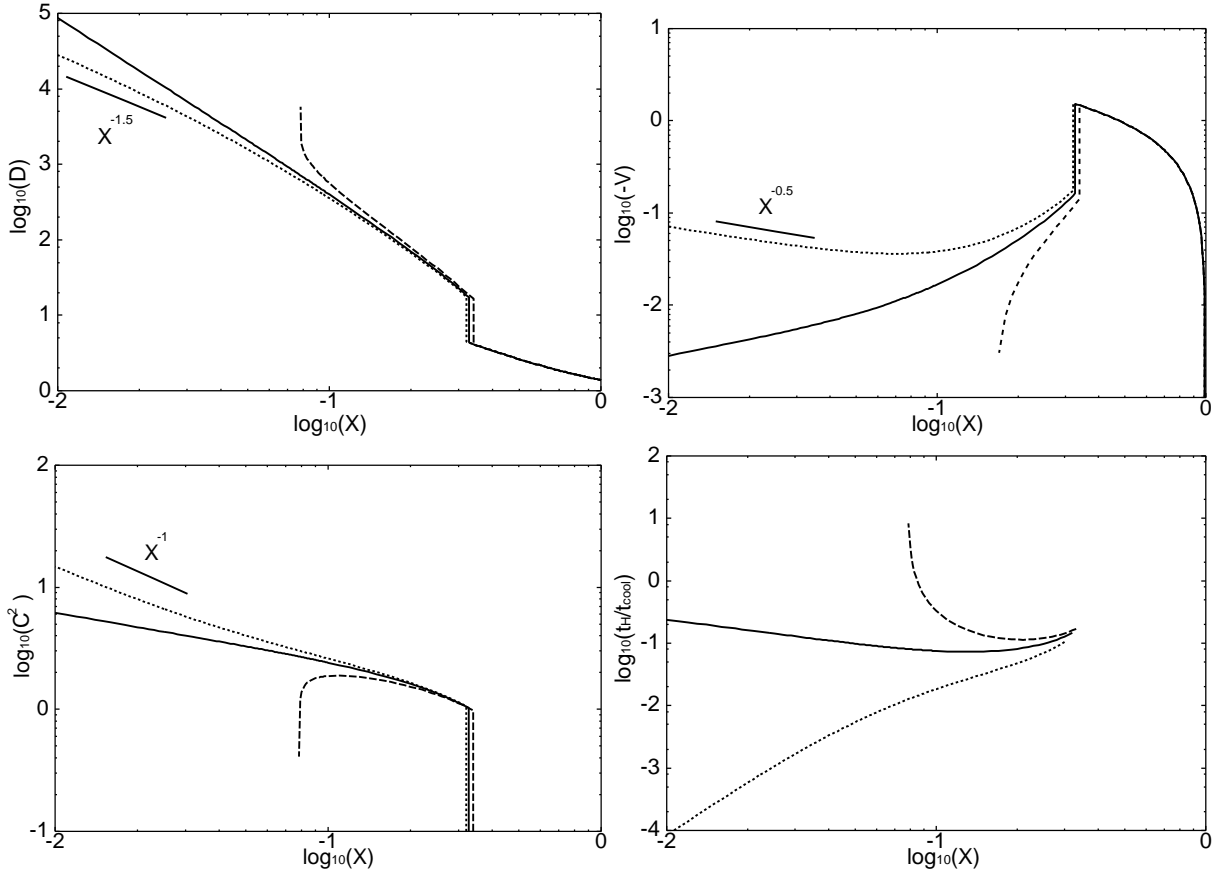


Figure 2. Three types of solutions with $\epsilon=1$ ($n=3$), $\mathcal{H}=0$, $A=2$, $B=-7/2$, and $K_0=0.01$. Each line shows the resultant profiles of the 'stagnation' solution (dashed line), 'eigensolution' (solid line), and 'adiabatic' solution (dotted line), respectively. The shock radii are $X_s=0.338976$, 0.326595 , and 0.3 , respectively. Each panel represents radial profiles of the density (top left), the proper velocity (top right), the square of the sound speed corresponding to the temperature (bottom left), and the ratio of the Hubble time to the cooling time (bottom right), respectively.

2.4 Numerical integration and boundary conditions

Assuming that the gas pressure is zero, the physical variables of a gas shell are given by the parameter θ (Peebles 1980):

$$X = \frac{r}{r_{ta}} = \sin^2\left(\frac{\theta}{2}\right) \left(\frac{\theta - \sin\theta}{\pi}\right)^{-\xi}, \quad (36)$$

$$D = \frac{9}{2} \frac{(\theta - \sin\theta)^2}{(1 - \cos\theta)^3 (1 + 3\epsilon\chi)}, \quad (37)$$

$$V = X \frac{\sin\theta(\theta - \sin\theta)}{(1 - \cos\theta)^2}, \quad (38)$$

$$C = 0, \quad (39)$$

$$M = \frac{9}{2} \frac{(\theta - \sin\theta)^2}{(1 - \cos\theta)^3} X^3, \quad (40)$$

with $\chi=1-3V/2X$. The outer boundary condition is defined at the turn-around radius, $\theta=\pi$. The collisional gas shell falls toward the center after the turn around, and the central gas density increases. Eventually, adiabatic compression occurs, and a shock propagates outward. The shock radius appears at a fixed fraction of the turn-around radius. The shock jump conditions are written as

$$D_2 = \frac{\gamma + 1}{\gamma - 1} D_1, \quad (41)$$

$$V_2 = \xi X_s + (V_1 - \xi X_s) \frac{\gamma - 1}{\gamma + 1}, \quad (42)$$

$$C_2^2 = \frac{2\gamma(\gamma - 1)}{(\gamma + 1)^2} (V_1 - \xi X_s)^2, \quad (43)$$

where subscripts 1 and 2 represent the pre- and post-shock quantities, and X_s is the non-dimensional shock radius. We need to determine the shock position. Bertschinger (1989) and Abadi et al. (2000) showed three types of solutions by changing the shock radius. Figure 2 represents the three possible solutions of the 'stagnation' solution (dashed line), 'eigensolution' (solid line), and 'adiabatic' solution (dotted line) for $\epsilon=1$ ($n=3$), $\mathcal{H}=0$, $A=2$, $B=-7/2$, and $K_0=0.01$. Each shock radius is $X_s=0.338976$, 0.326595 , and 0.3 , respectively. The ratio of the Hubble time to the cooling time at each radius is shown in Fig. 2, which is defined by

$$\frac{t_H}{t_{cool}} = K_0 D^{A-1} C^{2B-2}. \quad (44)$$

The first type is the 'stagnation' solution (dashed line), which diverges at a small radius. We found that the similarity solution with $X_s=0.338976$, which corresponds

to the shock position of Bertschinger's adiabatic solution (Bertschinger 1985), becomes the 'stagnation' solution. We analytically explain that the divergence at the small radius occurs due to cooling. Because the profiles of the fluid variables are not influenced by cooling in the outer region, we assume that the velocity approaches $V=V_0X$, which is the same as that of the adiabatic solution (Chuzhoy & Nusser 2000). The density and temperature can be expressed from equations (31) and (33) as follows:

$$D = D_0 X^s, \quad C = C_0 X^t, \quad (45)$$

where

$$s = \frac{1}{V_0 - \xi} (2 - 3V_0), \quad (46)$$

$$t = \frac{1}{V_0 - \xi} \left[-(\xi - 1) - \frac{K_0}{2} D^{A-1} C^{2B-2} - \frac{3}{2}(\gamma - 1)V_0 + \frac{\gamma(\gamma - 1)}{2} \mathcal{H} \right]. \quad (47)$$

As the gas relaxes to a hydrostatic equilibrium in order to vanish the velocity as $X \rightarrow 0$, $2t - s = 2$ is satisfied by equation (32), in which case V_0 is

$$V_0 = \frac{1}{3\gamma - 4} [-K_0 D^{A-1} C^{2B-2} + \gamma(\gamma - 1)\mathcal{H}]. \quad (48)$$

The first and second terms on the right-hand side represent the cooling and heating terms, respectively. We consider the behavior of the cooling term in the inner region in the case of $\mathcal{H}=0$. Assuming that the cooling term converges to zero at the center, $D^{A-1} C^{2B-2}$ becomes

$$D^{A-1} C^{2B-2} \propto X^\kappa, \quad (49)$$

where

$$\kappa = -\frac{2}{\xi}(A - 1) + \frac{\xi - 1}{\xi}(2B - 2) > 0. \quad (50)$$

However, the parameters A and B , which satisfy $\kappa > 0$, are not in the range of $0 < \epsilon \leq 1$. Thus, $\kappa < 0$ is satisfied and the first term on the right-hand side of equation (48) diverges, resulting in a steeper drop of the temperature. That is to say, a cooling catastrophe occurs in the inner region.

The second type is an 'adiabatic' solution (dotted line). It is a free-fall solution to a point mass. Thus, the density and velocity asymptotically approach $D \propto X^{-3/2}$ and $V \propto X^{-1/2}$, respectively. Because the cooling and heating times are longer than the flow time, they are negligible for $X \rightarrow 0$. For the law conservation of energy, the sound speed approaches $C \propto X^{-1/2}$ as $X \rightarrow 0$.

The third type of solution is the 'eigensolution' (solid line), which is a marginal case of 'stagnation' solutions. That is to say, the 'eigensolution' satisfies the condition $t_{\text{flow}} = t_{\text{cool}}$ at the origin. A divergence of the physical variables does not occur, and the flow extends to $X=0$. The 'eigensolution' is the only solution where the mass is zero at the origin. We only derive the 'eigensolution' below.

3 RESULTS

We derive the similarity solutions of various cases of (A, B) . The first case is $(A, B) = (3/2, 1)$, which is the same as Abadi et al. (2000). The others are focused on the free-free and line

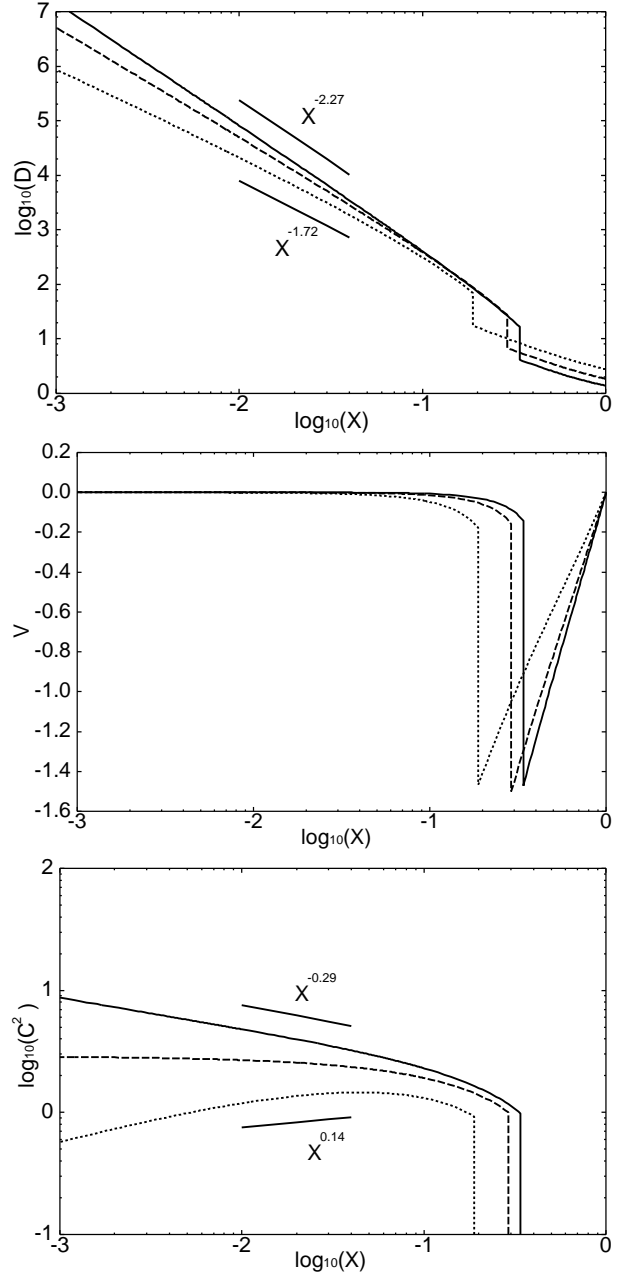


Figure 3. Similarity solutions without cooling and heating. Each line indicates the results of $\epsilon=1$ (solid line), $\epsilon=2/3$ (dashed line), and $\epsilon=1/3$ (dotted line), respectively. Each panel represents radial profiles of the density (top panel), the proper velocity (middle panel), and the square of the sound speed corresponding to the temperature (bottom panel), respectively.

emissions. As we can see from Fig. 1, the free-free and line emissions are out of the range $0 < \epsilon \leq 1$. Thus, we fix one parameter to $B=1/2$, $-1/2$, and $A=2$, in which case the other parameter, A or B , is obtained from equation (13).

3.1 Adiabatic solution

We first represent the solutions without cooling and heating for a comparison. Figure 3 shows the solutions for $\epsilon=1$

ϵ	X_s	u	v
1.0	0.338976	-2.27	-0.29
2/3	0.289976	-2.05	-0.09
1/3	0.188952	-1.72	+0.14

Table 1. Properties of similarity solutions without cooling and heating. X_s is the non-dimensional shock radius, u and v are the gradient of the density and the square of the sound speed corresponding to the temperature which are fitted from $X=0.01$ to 0.04.

(solid line), $\epsilon=2/3$ (dashed line), and $\epsilon=1/3$ (dotted line), respectively. Each shock radius is $X_s=0.338976$ for $\epsilon=1$, 0.289976 for $\epsilon=2/3$, and 0.188952 for $\epsilon=1/3$, respectively. $\epsilon=1/3(n=-1)$ is the closest to the slope of the CDM power spectrum on cluster scales (Tadros et al. 1998). Outside of the shock radius, the gas falls freely to the center. After passing through the shock front, the gas velocity becomes nearly zero, and the gas is approximately in a hydrostatic equilibrium. Chuzhoy & Nusser (2000) analytically obtained asymptotic slopes of the similarity variables, and found $D \propto X^{-3(n+3)/(n+5)}$ and $T \propto X^{-(n-1)/(n+5)}$ as $X \rightarrow 0$ in the case of $\epsilon > 1/6(n > -2)$. For $\epsilon=1$, 2/3, and 1/3, the density becomes $\propto X^{-2.25}$ for $\epsilon=1$, $\propto X^{-2}$ for $\epsilon=2/3$, and $\propto X^{-1.5}$ for $\epsilon=1/3$, and the temperature becomes $\propto X^{-0.25}$ for $\epsilon=1$, $\propto X^0$ for $\epsilon=2/3$, and $\propto X^{0.5}$ for $\epsilon=1/3$, respectively. From the results of a numerical calculation, we confirmed that their slopes do not match the analytic slopes because the velocity is not completely zero. Table 1 gives the shock radius X_s , as well as the slopes of density u and temperature v , which were fitted from $X=0.01$ to 0.04. In the case of $\epsilon=1/3$, the temperature shows a decreasing profile toward the center. The reason for this is the strength of the shock wave. Because the shock velocity is $v_s = dr/dt \propto t^{\xi-1}$, the shock wave becomes strong with time when $\xi > 1.0$ ($\epsilon < 2/3$), resulting in a decreasing temperature profile toward the center.

3.2 Case of $A=3/2$, $B=1$

We investigate the properties of solutions for $\Lambda \propto \rho^{3/2}T$, which is the same cooling function as that of Abadi et al. (2000). Figure 4 shows the resultant profiles for $K_0=0.01$ without heating, $\mathcal{H}=0$. Each line shows the results of $\epsilon=1$ (solid line), $\epsilon=2/3$ (dashed line), and $\epsilon=1/3$ (dotted line), respectively. Table 2 gives the shock radius X_s , and the slopes of the similarity variables which were fitted from $X=0.01$ to 0.04. Outside of the shock radius, the gas pressure is assumed to be zero. Thus, cooling and heating are neglected in this region. The fluid variables have the same shapes as the adiabatic similarity solution in Fig. 3. For $X < X_s$, the gas has almost hydrostatic distributions. However, in the inner region, where the radiative cooling time is less than the age, radiative cooling affects the gas distribution. As a result, the pressure support decreases, and a cooling inflow is established. In Fig. 4, the non-dimensional changes of the internal energy and the work done on a unit mass are shown,

ϵ	\mathcal{H}	X_s	u	v	w
$K_0=0.01$					
1.0	0	0.311328	-2.03	-0.81	-0.02
	0.4	0.385248	-1.88	-0.64	-0.36
	0.8	0.519181	-1.15	+0.60	+1.12
2/3	0	0.269172	-2.00	-0.67	+0.02
	0.4	0.320795	-1.79	-0.41	-0.42
	0.8	0.397242	-1.26	+0.50	+1.27
1/3	0	0.179164	-1.83	-0.27	+0.15
	0.4	0.199747	-1.64	+0.03	-0.02
	0.8	0.224469	-1.33	+0.38	+2.06
$K_0=0.1$					
1.0	0	0.185853	-2.01	-0.97	+0.002
	0.4	0.209495	-1.99	-0.96	+0.03
	0.8	0.247105	-1.96	-0.94	+0.06
2/3	0	0.154968	-2.00	-0.94	-0.001
	0.4	0.171938	-1.98	-0.93	-0.03
	0.8	0.197048	-1.95	-0.92	-0.06
1/3	0	0.099695	-1.97	-0.88	+0.003
	0.4	0.107732	-1.94	-0.87	+0.02
	0.8	0.118345	-1.92	-0.85	-0.06

Table 2. Properties of solutions for $\Lambda \propto \rho^{3/2}T$. \mathcal{H} is the parameter of heating, w is the slope of the velocity fitted from $X=0.01$ to 0.04, and the other parameters are the same as those given in Table 1.

which are defined by

$$\frac{dE}{dt} = \frac{r_{ta}^2}{t_H^3} \Theta, \quad (51)$$

$$\frac{-Pd(1/\rho)}{dt} = \frac{r_{ta}^2}{t_H^3} \Pi, \quad (52)$$

where P is the gas pressure. Using equations (21)-(24), the non-dimensional variables are given by

$$\Theta = \frac{2C^2}{\gamma(\gamma-1)} [\xi - 1 + \frac{V - \xi X}{C} \frac{dC}{dX}], \quad (53)$$

$$\Pi = \frac{C^2}{\gamma} [\frac{V - \xi X}{D} \frac{dD}{dX} - 2]. \quad (54)$$

In Fig. 4, the gas is compressed because $\Pi > 0$. More than 60 percent of the work is turned into internal energy, and the gas heats up. Since Θ increases with decreasing radius, the temperature increases with decreasing radius.

We discuss the slopes of the similarity variables, including cooling. In Fig. 4, the density slopes of $\epsilon=1$ and 2/3 are shallower than those of Fig. 3. For $\epsilon=1/3$, the density is steeper than the result of Fig. 3. On the other hand, the temperature increases with decreasing radius in all cases. Abadi et al. (2000) found that the slopes of the density and temperature approach -2 and -1 as $X \rightarrow 0$, respectively. In the case of (A, B) , assuming that the infall velocity is $V \ll -\xi X$ and approach $V = V_0 X^w$ as $X \rightarrow 0$, the density and sound speed are expressed from equations (31)-(33), and (35) as follows:

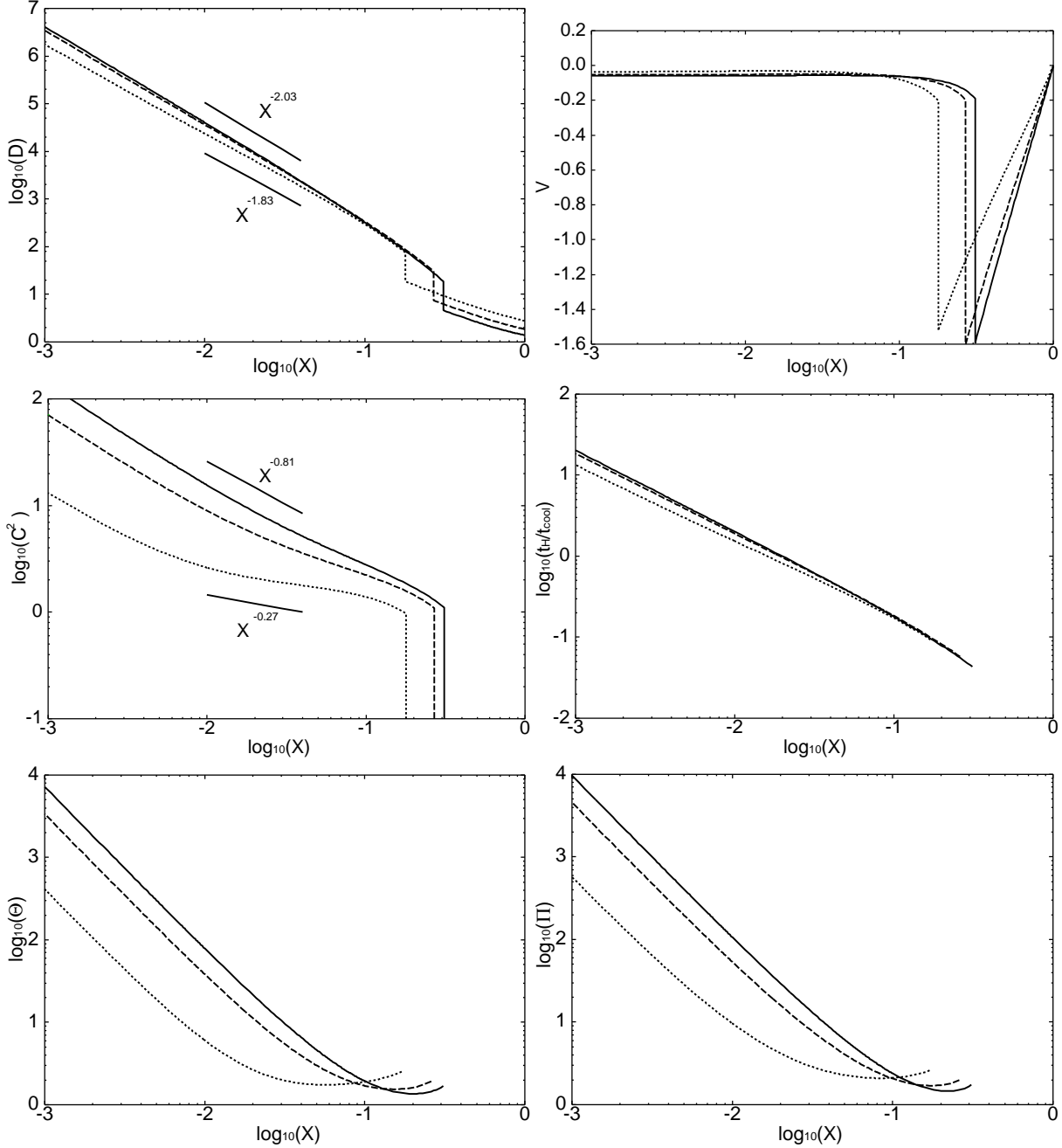


Figure 4. Similarity variables with $A=3/2$, $B=1$, $K_0=0.01$, and $\mathcal{H}=0$. Each line shows the solutions of $\epsilon=1$ (solid line), $\epsilon=2/3$ (dashed line), and $\epsilon=1/3$ (dotted line), respectively. Each panel indicates radial profiles of the density (top left), the proper velocity (top right), the square of the sound speed corresponding to the temperature (middle left), the ratio of the Hubble time to the cooling time (middle right), the change of internal energy on the unit mass (bottom left), and the work done on the unit mass (bottom right), respectively.

$$D = D_0 X^s, \quad C = C_0 X^t, \quad (55)$$

where

$$\begin{aligned} s &= \frac{w + B - 2}{A - 1} \quad (A \neq 1), \\ &= B - 4 \quad (A = 1), \end{aligned} \quad (56)$$

$$t = -\frac{1}{2}. \quad (57)$$

From Table 2, in the case of $K_0=0.1$, the infall velocity is ap-

proximately constant (i.e., $w=0$). Substituting $A=3/2$, $B=1$, and $w=0$ for equation (56), the density slope becomes -2 , and the temperature slope is -1 from equation (57). We can see from Table 2 that the density and temperature slopes of numerical calculations for $K_0=0.1$ are considerably close to -2 and -1 , respectively. In the case of $K_0=0.01$ without heating, the infall velocity is approximately constant. However, $V \ll -\xi X$ is not fully satisfied because the energy loss is smaller than that of $K_0=0.1$, in which case the gas distri-

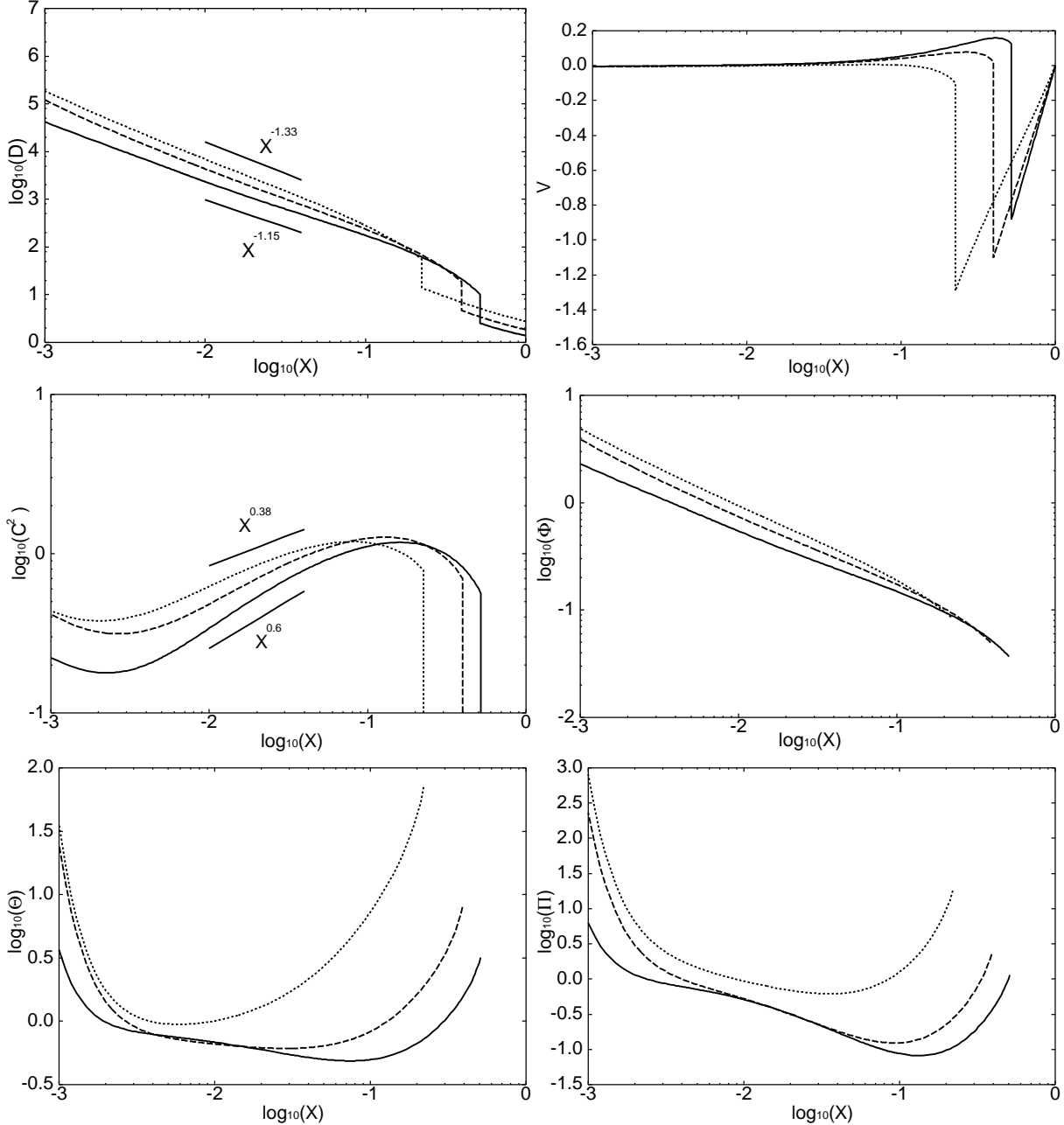


Figure 5. Similarity variables with $A=3/2$, $B=1$, $K_0=0.01$, and $\mathcal{H}=0.8$. The middle right panel indicates the ratio of the cooling rate to the heating rate, and the other panels are the same as in Fig. 4.

bution approaches the adiabatic one. Thus, the density and temperature slopes turn into the middle gradient between the case of $K_0=0.1$ and the adiabatic solution in Fig. 3.

Next, we represent the similarity solutions that incorporate the effects of heating and cooling. Figure 5 shows the resultant profiles for $\mathcal{H}=0.8$, and the other parameters have the same values as in the previous model. We show the ratio Φ of the cooling rate to the heating rate,

$$\Phi = \frac{\Lambda}{\Gamma} = \frac{K_0}{\mathcal{H}\gamma(\gamma-1)} D^{A-1} C^{2B-2}. \quad (58)$$

Since the heating rate is greater than the cooling rate behind the shock, the infall velocity is weakened by heating,

and the gas expands because $\Pi < 0$ and cools down as $\Theta < 0$. The slope of the density becomes substantially shallow compared with the result of no heating, shown in Fig. 4, because the concentration of mass is suppressed due to heating. On the other hand, temperature increases with decreasing radius for $X > 0.1$. However, the change of internal energy (Θ) steeply decreases with decreasing radius, except in the central region. As a result, in $X=0.003 \sim 0.1$, the temperature becomes decreasing profiles toward the center. When the flow approaches the central region, the cooling rate becomes greater than the heating rate. In this region, radiative cooling produces a cooling inflow, the velocity becomes negative

ϵ	A, B	\mathcal{H}	X_s	u	v	w
$K_0=0.01$						
1.0	14/9, 1/2	0	0.318480	-2.19	-0.69	+0.16
		0.8	0.512580	-1.34	+0.34	+2.52
2/3	3/2, 1/2	0	0.277630	-2.11	-0.44	+0.24
		0.8	0.397755	-1.26	+0.46	+1.64
1/3	4/3, 1/2	0	0.186403	-1.79	+0.08	+1.06
		0.8	0.229463	-1.11	+0.44	+0.86
1.0	5/3, -1/2	0	0.323424	-2.31	-0.54	+0.38
		0.8	0.496057	-1.71	-0.07	-1.36
2/3	3/2, -1/2	0	0.283470	-2.12	-0.23	+0.55
		0.8	0.398342	-1.25	+0.40	+2.61
1/3	1.0, -1/2	0	0.188644	-1.73	+0.14	+1.47
		0.8	0.232110	-1.00	+0.42	+0.94
$K_0=0.1$						
1.0	14/9, 1/2	0	0.230693	-2.23	-0.91	+0.22
		0.8	0.307894	-2.14	-0.86	+0.10
2/3	3/2, 1/2	0	0.210950	-2.25	-0.82	+0.29
		0.8	0.273013	-2.14	-0.74	+0.13
1/3	4/3, 1/2	0	0.166035	-2.10	-0.30	+0.56
		0.8	0.201210	-1.76	-0.02	+0.13
1.0	5/3, -1/2	0	0.262117	-2.48	-0.77	+0.54
		0.8	0.334214	-2.35	-0.71	+0.32
2/3	3/2, -1/2	0	0.247433	-2.38	-0.52	+0.65
		0.8	0.313539	-2.16	-0.36	+0.15
1/3	1.0, -1/2	0	0.185988	-1.76	+0.11	+1.36
		0.8	0.226802	-1.11	+0.42	+0.88

Table 3. Properties of solutions which fixed the temperature dependence of the radiative cooling functions to $B=1/2$ or $-1/2$. The other parameters are the same as those given in Table 2.

and the gas is compressed. Because the change of the internal energy (Θ) shows a steeper rise toward the center in $X<0.003$, the gas heats up and the temperature shows increasing profiles toward the origin.

For the case of $K_0=0.1$, we can see from Table 2 that the slopes of the density and the temperature do not change significantly by increasing the coefficient of heating, \mathcal{H} , and are about -2 and -1 , respectively. The reason is that the flows are not affected by heating because the cooling is stronger than heating at all radii.

3.3 Cases of $B=1/2$, or $-1/2$

We derive the similarity solutions fixed to $B=1/2$ or $-1/2$. The former is similar to the temperature dependence of free-free emission. Since A is determined by equation (13), $A=14/9$ for $\epsilon=1$, $A=3/2$ for $\epsilon=2/3$, and $A=4/3$ for $\epsilon=1/3$, respectively. The latter is similar to the temperature dependence of the line emission. Similarly, $A=5/3$ for $\epsilon=1$, $A=3/2$ for $\epsilon=2/3$, and $A=1$ for $\epsilon=1/3$, respectively. Because

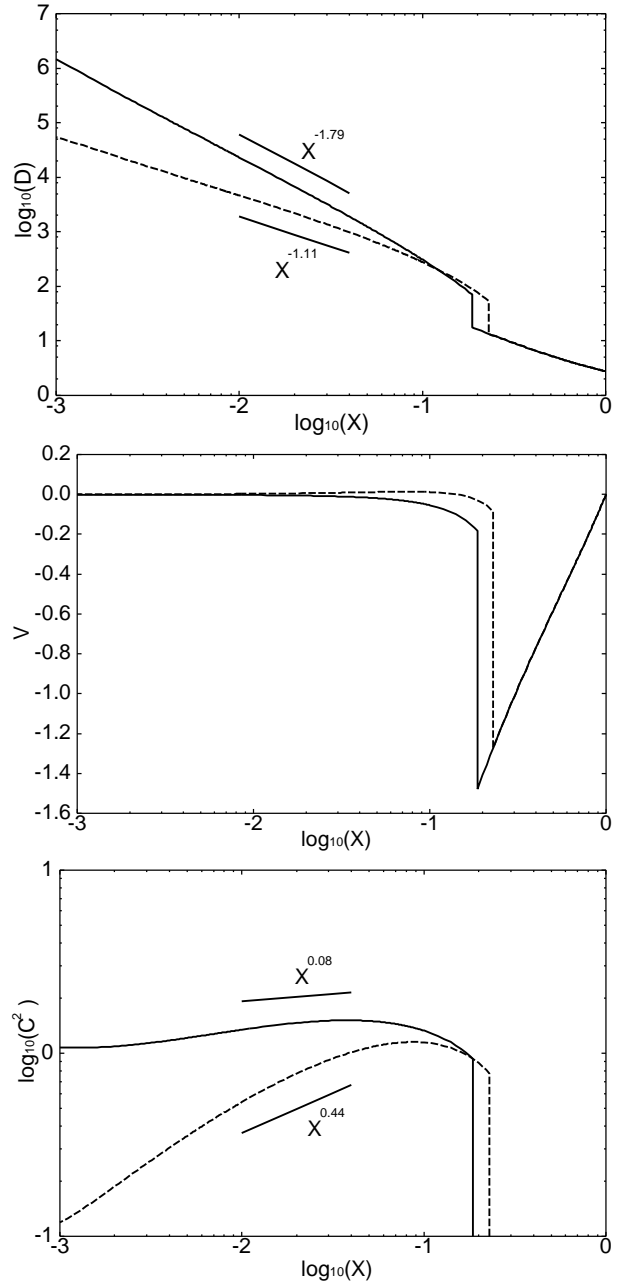


Figure 6. Similarity variables with $\epsilon=1/3$ ($n=-1$), $A=4/3$, $B=1/2$, and $K_0=0.01$. The solid and dashed lines indicate the results without heating, $\mathcal{H}=0$, and with heating, $\mathcal{H}=0.8$, respectively. Each panel represents radial profiles of the density (top panel), the proper velocity (middle panel), and the square of the sound speed corresponding to the temperature (bottom panel), respectively.

the realistic free-free and line emissions are proportional to the square of the density, $A=2$, the energy loss of the cooling functions assumed here is less than that of the realistic one. Figures 6 and 7 show the solutions of $(A, B)=(4/3, 1/2)$ and $(1, -1/2)$ with $\epsilon=1/3$ ($n=-1$) and $K_0=0.01$, respectively. The solid and dashed lines display the solutions without heating, $\mathcal{H}=0$, and with heating, $\mathcal{H}=0.8$, respectively. The shock radius X_s , and the slopes of the similarity variables

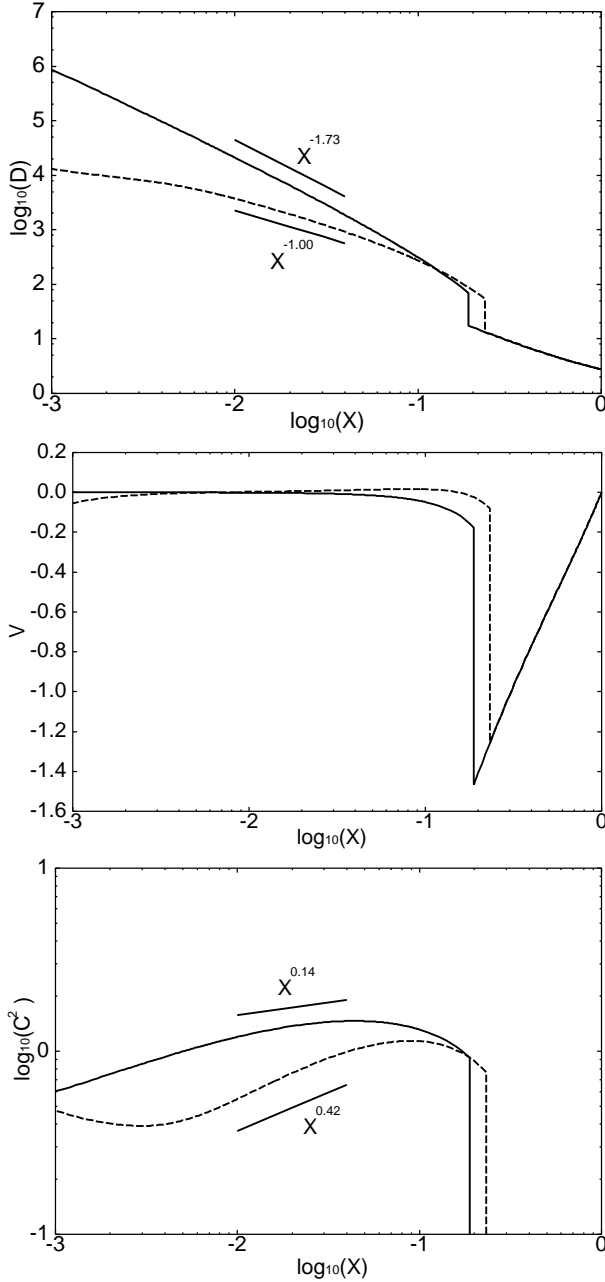


Figure 7. Same as in Fig. 6, except $A=1$ and $B=-1/2$.

are given in Table 3. For $\epsilon=1/3$, the energy loss of cooling is small because $A=3/4$ and 1. Thus, the density and temperature without heating are almost the same profiles as the adiabatic solutions in Fig. 3. For the heating solution with $\mathcal{H}=0.8$, the slope of the density becomes shallow and the temperature is lower than that of no heating, $\mathcal{H}=0$. The main reason is the same as the previous discussion in Section 3.2.

From Table 3, for $\epsilon=1$ and $2/3$ in the case of $K_0=0.1$, the density slopes are steeper than those of $\Lambda \propto \rho^{3/2}T$. If the infall velocity is $V \ll -\xi X$, the slope of temperature approaches -1 , from equation (57). On the other hand, the density slope depends on the values of A , B , and the slope

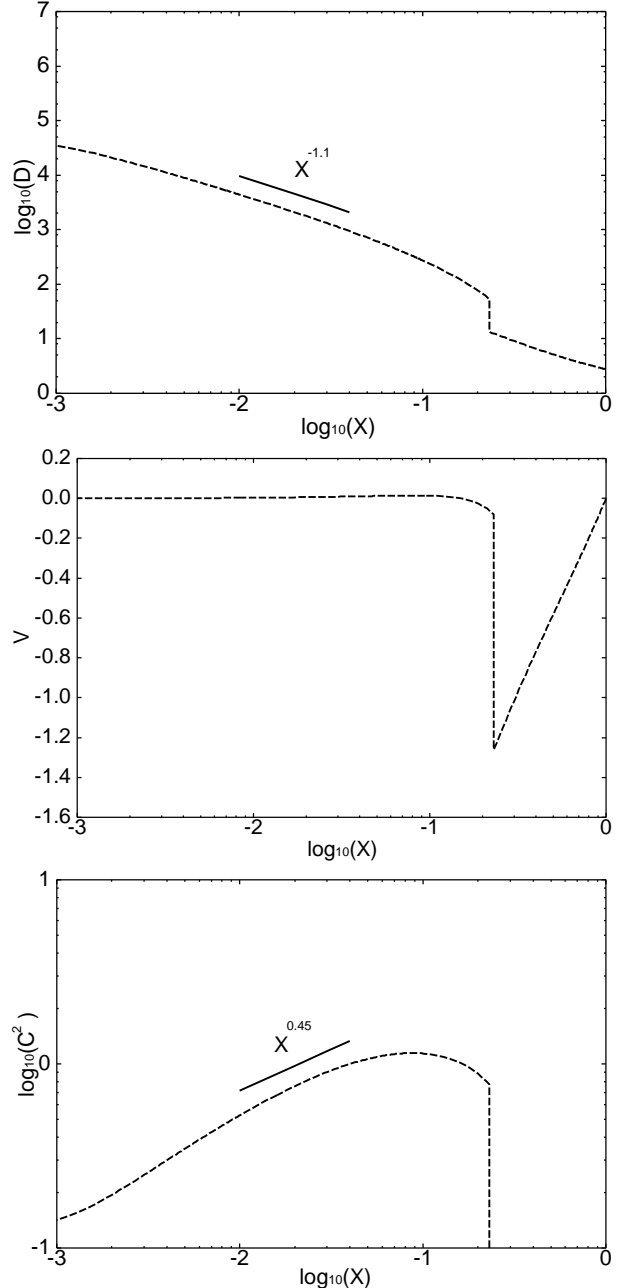


Figure 8. Similarity variables with $A=2$, $B=5/2$, and $K_0=10^{-4}$. The dashed line indicates the result with heating, $\mathcal{H}=0.8$. The panels indicate the same variable as in Fig. 6.

of velocity w from equation(56). For example, substituting $(A, B, w) = (14/9, 1/2, 0.22)$ and $(5/3, -1/2, 0.54)$, which is the case of $\epsilon=1$ with $K_0=0.1$, for equation (56), the density slopes become -2.3 and -2.94 , respectively. The resultant slope of the numerical calculation is shallower than this slope because $V \ll -\xi X$ is not fully satisfied.

3.4 Two-particle processes, $A=2$

We consider the similarity solutions for the case that cooling function has a collisional process, $A=2$. We exclude the case

ϵ	\mathcal{H}	X_s	u	v	w
$K_0=0.01$					
	0	0.326595	-2.32	-0.39	+0.63
1.0	0.4	0.378087	-2.13	-0.29	-0.70
	0.8	0.438560	-1.93	-0.28	-0.61
$K_0=0.1$					
	0	0.283055	-2.48	-0.52	+0.91
1.0	0.4	0.304111	-2.36	-0.47	+0.59
	0.8	0.323845	-2.06	-0.51	-0.06

Table 4. Same as Table 2, except $A=2$ and $B=-7/2$.

K_0	\mathcal{H}	X_s	u	v	w
10^{-4}	0.7	0.224706	-1.23	+0.42	+0.80
	0.8	0.231401	-1.10	+0.45	+0.82
10^{-5}	0.5	0.214030	-1.32	+0.36	+0.52
	0.8	0.232478	-0.91	+0.33	+0.20
10^{-6}	0.3	0.203330	-1.49	+0.28	+6.24
	0.8	0.232689	-0.96	+0.39	+1.18

Table 5. Properties of solutions for $\epsilon=1/3(n=-1)$, $A=2$, and $B=5/2$. The parameters are the same as those given in Table 2.

of $\epsilon=2/3$ because of $A=3/2$ from equation (13). Thus, we derive the similarity solutions with $\epsilon=1$ and $1/3$. For $\epsilon=1$, $B=-7/2$. Table 4 gives the results of the slopes of the similarity variables. The density profiles are steeper than those of $\Lambda \propto \rho^{3/2} T$. Substituting $(A, B, w) = (2, -7/2, 0.91)$, which is the case of $K_0=0.1$ and $\mathcal{H}=0$, for equation (56), the density slope becomes -4.59 , and the temperature slope becomes -1 from equation (57). However, because $B=-7/2$, the energy loss is not large enough to produce a large infall velocity. As a result, the gradients of the density and temperature become about -2.5 and -0.5 in the case of $K_0=0.1$.

For $\epsilon=1/3(n=-1)$, the cooling function is $\Lambda \propto \rho^2 T^{5/2}$, in which case we only find the 'stagnation' solution in the cases of $K_0=0.01$ or 0.1 . The reason is that the effect of cooling is very strong at the central region, leading to a cooling catastrophe. Therefore, we try to find heating solutions that can balance the cooling. As a result, when $K_0=10^{-4}$, we find that the heating solutions exist with $\mathcal{H}=0.7-0.8$, and that the heating is so weak that a cooling catastrophe is unavoidable in the case of $\mathcal{H} < 0.7$. Similarly, when $K_0=10^{-5}$, an 'eigensolution' exists with $\mathcal{H}=0.5-0.8$. When $K_0=10^{-6}$, we find an 'eigensolution' with $\mathcal{H}=0.3-0.8$. Table 5 gives its properties. When $K_0 > 10^{-4}$ and $\mathcal{H} > 0.8$, the heating is strong in the outer region where cooling can be neglected, and the expanding velocity becomes large and an 'eigensolution' is not found. Figure 8 shows the result of $\epsilon=1/3$, $K_0=10^{-4}$, and $\mathcal{H}=0.8$. Because the effect of heating is strong in the outer region, the slope of the density becomes shallow and the

temperature decreases with decreasing radius, which are the same reasons as described for the previous model discussed in Section 3.2.

4 DISCUSSION AND SUMMARY

In this paper, we present self-similar solutions including cooling and heating for collisional gas. We assume that the cooling rate has a power-law dependences of the gas density and temperature, $\Lambda \propto \rho^A T^B$, and that the heating rate is $\Gamma \propto \rho T$. In order to obtain a similarity solution, A and B are selected by requiring that the cooling time is proportional to the dynamical time. The main results in this paper are the following:

(i) In the region where the cooling rate is stronger than the heating rate, a cooling inflow is established, and the gas is compressed and heats up. Because the compression is stronger in the inner region than in the outer region, the temperature increases with decreasing radius. Furthermore, if the large infall velocity, $V \ll -\xi X$, is produced due to an enormous energy loss, the temperature slope approaches -1 , and the density slope approaches a value that depends on A , B , and the velocity slope w .

(ii) In the region where the heating rate is larger than the cooling rate, the infall velocity is suppressed by heating, the compression is weakened and the gas cools down. The slope of the density becomes shallow due to suppression of the collapse, and the temperature is lower than that without heating.

(iii) For $\epsilon=1/3$ ($n=-1$) and $(A, B)=(2, 5/2)$, the 'stagnation' solutions are only derived in the cases of $K_0=0.1$ or 0.01 . The reason for this is that the cooling is very strong in the inner region, and a cooling catastrophe occurs. We include the heating and a small K_0 in order to decrease the effect of cooling, and find heating solutions that can balance the cooling with $K_0=10^{-4}$ and $\mathcal{H}=0.7-0.8$.

We consider that the self-similarity solution presented here can be used for modeling of structure formations. For example, the value of the slope parameter, β_{fit} , obtained from observations of the surface brightness profile indicates the typical value for rich clusters, $\beta_{fit} \sim 2/3$. On the other hand, group systems have significantly flatter slopes with $\beta_{fit} \sim 0.4$ (Arnaud & Evrard 1999; Helsdon & Ponman 2000). As an origin of such discrepancies, it has been proposed that the intracluster medium (ICM) extends to the outer regions by non-gravitational heating, leading to flatter density profiles (Metzler & Evrard 1997). Furthermore, in the model $A=2$ and $\epsilon=1/3(n=-1)$, which is close to those of real clusters, a cooling catastrophe occurs if there is no heating, and there are the heating solutions that can balance the cooling. This may mean that real clusters oscillate between a heating dominated regime and one with a cooling catastrophe (Kaiser & Binney 2003), or that the heating sources, such as AGN (Churazov et al. 2001; Quilis et al. 2001; Reynolds et al. 2002; Brüggen et al. 2002; Brüggen & Kaiser 2002; Brüggen 2003) or thermal conduction (Fabian et al. 2002; Ruszkowski & Begelman 2002; Voigt et al. 2002; Zakamska & Narayan 2003), balance the cooling. Of course, it is difficult to directly apply the solution presented here to a real cluster, because the time evolutions of the cooling and

heating differ from the Hubble time. For a realistic treatment of this problem, it is necessary to perform a numerical simulation while assuming regular radiative cooling and heating rates. However, the accuracy of the numerical simulation is limited by the finite resolution. We consider that a comparison between the simulation and the similarity solution gives insights into the thermal evolution of clusters of galaxies.

ACKNOWLEDGMENTS

We would like to thank an anonymous referee for very useful comments and suggestions, which have improved the quality of our work.

REFERENCES

Abadi M.G., Bower R.G., Navarro J.F., 2000, MNRAS, 314, 759
 Arnaud M., Evrard A.E., 1999, MNRAS, 305, 631
 Bertschinger E., 1985, ApJS, 58, 39
 Bertschinger E., 1989, ApJ, 340, 666
 Brüggen M., Kaiser C.R., Churazov E., Enßlin T.A., 2002, MNRAS, 331, 545
 Brüggen M., Kaiser C.R., 2002, Nature, 418, 301
 Brüggen M., 2003, ApJ, 592, 839
 Churazov E., Brüggen M., Kaiser C.R., Böhringer H., Forman W., 2001, ApJ, 554, 261
 Chuzhoy L., Nusser A., 2000, MNRAS, 319, 797
 Evrard A.E., Henry J.P., 1991, ApJ, 383, 95
 Fabian A.C., Voigt L.M., Morris R.G., 2002, MNRAS, 335, L71
 Fillmore J.A., Goldreich P., 1984, ApJ, 281, 1
 Helsdon S.F., Ponman T.J., 2000, MNRAS, 315, 356
 Kaiser N., 1991, ApJ, 383, 104
 Kaiser C.R., Binney J., 2003, MNRAS, 338, 837
 Metzler C.A., Evrard A.E., 1997, astro-ph/9710324
 Owen J.M., Weinberg D.H., Villumsen J.V., 1998, astro-ph/9805097
 Peebles P.J.E., 1980, *The Large-Scale Structure of the Universe*. Princeton Univ. Press, Princeton
 Peterson J.R., Puerls F.B.S., Kaastra J.S., Arnaud M., Reiprich T.H., Fabian A.C., Mushotzky R.F., Jernigan J.G., Sakelliou I., 2001, A&A, 365, L104
 Quilis V., Bower R.G., Balogh M.L., 2001, MNRAS, 328, 1091
 Reynolds C.S., Heinz S., Begelman M.C., 2002, MNRAS, 332, 271
 Ruszkowski M., Begelman M.C., 2002, ApJ, 581, 223
 Tadros H., Efstathiou G., Dalton G., 1998, MNRAS, 296, 995
 Tamura T., Kaastra J.S., Peterson J.R., Puerls F.B.S., Mit-taz J.P.D., Trudolyubov S.P., Stewart G., Fabian A.C., Mushotzky R.F., Lumb D.H., Ikebe Y., 2001, A&A, 365, L87
 Voigt L.M., Schmidt R.W., Fabian A.C., Allen S.W., Johnstone R.M., 2002, MNRAS, 335, L7
 Zakamska N.L., Narayan R., 2003, ApJ, 582, 162

This paper has been produced using the Royal Astronomical Society/Blackwell Science L^AT_EX style file.